

Original Research

# Novel Prognostic Model Construction of Tongue Squamous Cell Carcinoma Based on Apigenin-Associated Genes

Jianfei Lai<sup>1,2</sup>, Chen Fang<sup>1,2</sup>, Guohua Zhang<sup>1,2</sup>, Chao Shi<sup>1,2</sup>, Feng Yu<sup>1</sup>, Weiguo Gu<sup>1</sup>,  
Jianxiong Deng<sup>1</sup>, Jingbiao Xu<sup>1</sup>, Chaoxing Liu<sup>1,2</sup>, Feng Qiu<sup>1,3,\*</sup><sup>1</sup>Department of Oncology, Gaoxin Branch of the First Affiliated Hospital, Jiangxi Medical College, Nanchang University, 330000 Nanchang, Jiangxi, China<sup>2</sup>Department of Oncology, The First Affiliated Hospital, Jiangxi Medical College, Nanchang University, 330000 Nanchang, Jiangxi, China<sup>3</sup>Nanchang Key Laboratory of Tumor Gene Diagnosis and Innovative Treatment Research, Gaoxin Branch of the First Affiliated Hospital, Jiangxi Medical College, Nanchang University, 330000 Nanchang, Jiangxi, China\*Correspondence: [ndyfy01149@ncu.edu.cn](mailto:ndyfy01149@ncu.edu.cn) (Feng Qiu)

Academic Editor: Francesca Diomedea

Submitted: 20 August 2023 Revised: 7 October 2023 Accepted: 24 November 2023 Published: 6 February 2024

## Abstract

**Background:** Clinical indexes are often selected as relevant factors for constructing prognostic models of tongue squamous cell carcinoma (TSCC) patients, while factors related to therapeutic targets are less frequently included. As Apigenin (API) shows anti-tumor properties in many tumors, in this study, we construct a novel prognostic model for TSCC patients based on Apigenin-associated genes through transcriptomic analysis. **Methods:** The effect of Apigenin (API) on the cell characteristics of TSCC cells was measured by several phenotype experiments. RNA-seq was executed to ensure differentially expressed genes (DEGs) in squamous cell carcinoma-9 (SCC-9) cells after API treatment. Furthermore, reverse transcription quantitative polymerase chain reaction (RT-qPCR) and immunohistochemistry were performed to verify the expression of API-related genes. Then, combined with the gene expression data and relevant individual information of TSCC samples acquired from The Cancer Genome Atlas (TCGA), an API-related model was built through Lasso regression and multivariate Cox regression. A receiver operating characteristic (ROC) curve and a nomogram and calibration curve were created to forecast patient outcomes to improve the clinical suitability of the API-related signature. The relationships between the two risk groups and function enrichment, immune infiltration characteristics, and drug susceptibility were analyzed. **Results:** We demonstrated that API could inhibit the malignant behavior of TSCC cells. Among API-related genes, TSCC cells treated with API, compared to the control group, have higher levels of transmembrane protein 213 (TMEM213) and G protein-coupled receptor 158 (GPR158), and lower levels of caspase 14 (CASP14) and integrin subunit alpha 5 (ITGA5). An 7 API-associated gene model was built through Lasso regression and multivariate Cox regression that could direct TSCC prognostic status and tumor immune cell infiltration. In addition, we acquired 6 potential therapeutic agents for TSCC based on the prognostic model. **Conclusions:** Our research suggested the inhibition effect of API on TSCC cells and provided a novel prognostic model combined with therapeutic factors that can guide the prognosis of TSCC and clinical decision-making in TSCC.

**Keywords:** Apigenin; TSCC; prognosis; prognostic model

## 1. Introduction

Apigenin (4',5,7-trihydroxyflavone, API), a plant flavonoid, has multiple antioxidant, anti-inflammatory, and anticancer activities [1–3]. In Europe, plant preparations containing API have been used for centuries as traditional medicines and are commonly used in the treatment of asthma, insomnia, neuralgia, herpes zoster, Parkinson's disease, and degenerative disorders [4–6]. Moreover, API can effectively inhibit various pathways that are important for the growth of tumors, including breast, skin, and colon cancers [3,7–9]. In breast cancer, API reduces estrogen receptor (ER)-positive cancer cell growth via protein kinase B (PKB)/Forkhead box protein M1 (FOXO1) molecular mechanisms [10]. Furthermore, in SKH-1 mouse models, API was demonstrated to inhibit Ultraviolet B (UVB)-induced carcinogenesis [11,12]. Moreover, API could ef-

fectively induce apoptosis in colon carcinoma cells and tongue squamous cell carcinoma (TSCC) [8,13]. *In vitro*, API inhibits the development of oral squamous cell carcinoma by causing apoptosis and cell cycle arrest [13]. However, its potential application in TSCC has not yet been fully investigated.

TSCC, which is associated with an aggressive phenotype and poor prognosis, is one of the most widely diagnosed forms of oral cancer [14–16]. In addition to functional problems such as impaired speech, chewing, and swallowing, TSCC may also cause cosmetic changes, which can reduce patients' quality of life [17,18]. Currently, the treatment of TSCC includes surgery, chemotherapy, radiotherapy, or comprehensive treatment depending on the patient's condition [4]. Although great improvement has been made in cancer diagnosis and therapy, the mortal-



ity of TSCC is still high [19]. Previous data have shown that the 5-year survival rate for patients with advanced TSCC is under 50%. Hence, more effective targets and therapies are desperately needed for TSCC [20]. And it's necessary to build new methods to predict TSCC prognosis.

Nowadays, prognostic models are being used extensively in predicting tumor prognosis. Multiple factors are included in the prognostic modeling because using some single prognostic factor alone is not accurate enough [21]. Among these factors, clinical biochemical and imaging indicators are the main components. Previous studies have demonstrated that in patients with N-type breast cancer, prognostic models can provide evidence for withholding chemotherapy when the prognosis is favorable [22]. In metastatic biliary tract cancer, prognostic models based on clinical-laboratory parameters can help to accurately risk-stratify patients and make treatment-related decisions [23]. Moreover, prognostic models using the neutrophil-to-lymphocyte ratio (NLR) and 18F-FDG PET standardized uptake values can identify patients with pancreatic cancer into 4 prognostically distinct risk groups [24]. However, the analysis of high-throughput data and the incorporation of therapeutic factors as prognostic factors in the construction of prognostic models are rare. Indeed, such an approach is more likely to assess the impact of treatment on the disease and to regulate the dose and duration of drug administration.

In this study, we aimed to prove the potential role of API in TSCC and explore a novel TSCC prognosis model. The prognostic model, based on API-associated genes, was effective in guiding TSCC prognosis and immune microenvironment.

## 2. Materials and Methods

### 2.1 Workflow

Firstly, API-related differentially expressed genes (DEGs) in squamous cell carcinoma-9 (SCC-9) cells were identified through RNA-seq and a preliminary analysis was conducted on the molecular mechanism of possible action of Apigenin. Next, combined with relevant individual information of TSCC patients from The Cancer Genome Atlas (TCGA) databases, 7 API-related genes were found to create a prognostic model and to survey the underlying mechanisms of TSCC patients [25]. The low- and high-risk groups were constructed to estimate patients' outcomes by accurately predicting their overall survival (OS) from TSCC. Furthermore, this model was used to classify the tumor microenvironment (TME) and drug sensitivity of TSCC patients in different risk groups. A schematic of the analysis workflow is demonstrated (Fig. 1).

### 2.2 Cell Line and Treatments

The TSCC cell lines SCC-9 and CAL-27 were purchased from the American Type Culture Collection (ATCC). For culturing, SCC-9 cells were grown in DMEM-F12 maintained at 37 °C with 5% CO<sub>2</sub>. And CAL-27

cells were cultured in DMEM medium in the same environment. All cell lines were validated by STR profiling and tested negative for mycoplasma. For experimental studies, SCC-9 and CAL-27 cells were treated with or without API (IA0400, Solarbio, Beijing, China) for the indicated period with dimethyl sulfoxide (DMSO, D8371, Solarbio, Beijing, China) as the vehicle. None of the final concentrations of DMSO in the medium exceeded 0.1% in all treatments.

### 2.3 Investigation of the IC<sub>50</sub> of API in TSCC Cells

The semi-inhibitory concentration (IC<sub>50</sub>) of API was calculated by the Cell Counting Kit-8 (CCK-8) assay (BA00208, Bioss, Beijing, China). In brief, 100 μL of SCC-9 and CAL-27 cells growing exponentially at a concentration of  $5 \times 10^4$  cells/mL were seeded into 96-well plates and further incubated with different concentrations of API (0, 2, 4, 8, 16, 32, 64, 128 μmol/L). After 24 hours, the CCK-8 chemical agent (10 μL) was mixed in each well, and the mixtures were incubated at 37 °C for 120 minutes. The OD values were tested at a wavelength of 450 nm. The IC<sub>50</sub> was determined by Prism 9 software (GraphPad Software, San Diego, USA).

### 2.4 Cell Proliferation Assays

SCC-9 and CAL-27 cells ( $3 \times 10^3$ ) in 100 μL of medium were inoculated into 96-well plates. Following the CCK-8 assay procedure, cell proliferation was analyzed at 1, 2, 3, 4, and 5 days. At the specified point in time, 10 μL of CCK-8 reagent was added to every well. After incubating for 2 h at 37 °C, a wavelength of 450 nm was used to analyze the OD values in each well, and growth curves were created to define the growth rates.

### 2.5 Wound-Healing Assay

Using a 200 μL pipette tip, a scratch was made in the center of each well. Each well was washed 3 times with PBS to remove cell debris. Then, the residual cells were treated with or without 20 μM API for 24 h. The migrating cells were imaged at 0 or 24 h by using a Leica inverted microscope (DMI8, Leica, Solms, Germany; magnification, 50×).

### 2.6 Transwell Migration and Invasion Assay

In the invasion assay, transwells were pretreated with matrigel (1:8). Following the suspension of SCC-9 and CAL-27 cells in serum-free medium ( $10 \times 10^5$ /mL), 200 μL of the cell suspension containing API (0, 5, 10 μM) were added to the upper compartment, and 800 μL of medium containing 20% fetal bovine serum (FBS) were used in the lower chamber. Then, SCC-9 cells were incubated for 24 hours in migration and 48 hours in invasion. As for CAL-27, cells were incubated for 48 hours in migration and 72 hours in invasion. Cells that had migrated were then fixed with 4% paraformaldehyde, followed by crystal violet staining. The number of migrating cells was determined after the cell chamber was photographed using a microscope (DMI8, Leica, Solms, Germany; magnification, 50×).

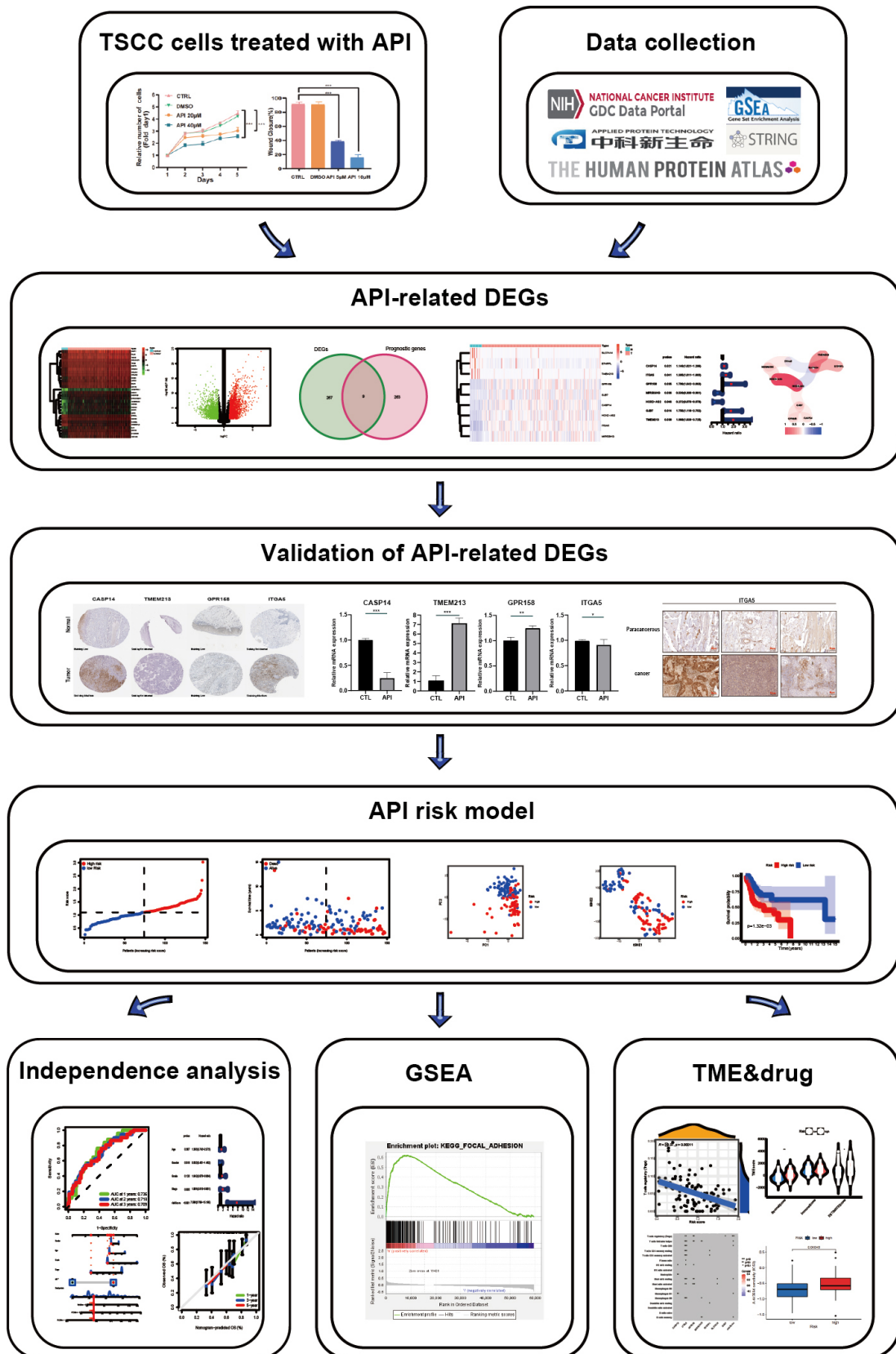


**Fig. 1. Analysis workflow.** TSCC, tongue squamous cell carcinoma; API, apigenin; DEGs, differentially expressed genes; GSEA, gene set enrichment analysis; TME, tumor microenvironment.

## 2.7 Colony Formation Assay

Six-well plates were used to cultivate SCC-9 and CAL-27 cells (1000/well). 20  $\mu$ M API was applied to the cells. And every three days, the culture medium was changed. After 10 days of incubation, cells were immobilized with 4% paraformaldehyde. Then, the cells were followed by 10 minutes of crystal violet staining. A digital camera was used to record colony images, and colonies with more than 50 cells each were tallied.

## 2.8 Immunohistochemistry (IHC)

Sections were cut from formalin-fixed, paraffin-embedded adjacent noncancerous tissues and cancer tissues. The sections were routinely deparaffinized, rehydrated, antigen-retrieved, and blocked with 3% hydrogen peroxide. Thereafter, primary antibodies for ITGA5 (1:200, Proteintech) were incubated on the sections overnight at 4 °C, followed by secondary antibodies that were HRP-labeled. The sections were stained with hematoxylin and then with diaminobenzidine. Unaware of any clinical information about our patients, two skilled pathologists independently evaluated and scored the stained sections based on the degree of staining and the ratio of tumor cells with a positive stain. The staining intensity has been separated into four groups: 0 for no staining, 1 for mild staining, 2 for moderate staining, and 3 for intense staining. The proportion of positively stained tumor cells was classified depending on the following criteria. 0 (5% positive cancer cells), 1 (5–25% positive cancer cells), 2 (26–50% positive cancer cells), 3 (>50% positive cancer cells). The total score is derived from the sum of the staining intensity and the stained cell score. Based on the total score, patients were separated into two groups: 0–2 negative and 3–6 positive.

## 2.9 Data collection

Transcriptome RNA sequencing data from SCC-9 cells treated with or without 20  $\mu$ M API for 24 hours were provided by Applied Protein Technology. RNA-seq data of TSCC patients obtained from the TCGA contained 148 TSCC samples and 15 normal tissue samples. Clinical data in 147 samples, including age, sex, tumor grade, and survival status, were also gathered from the TCGA. Besides, data from 58 additional samples were downloaded on the Gene Expression Omnibus database (<https://www.ncbi.nlm.nih.gov/geo/>) (ID: GSE111395, GSE75540), which later was used as a test cohort.

## 2.10 Establishment of the Prognostic Model

The “limma” package, containing  $p$  as well as false discovery rate (FDR) <0.05 as the cutoff points, was employed to detect DEGs between tumor tissues and normal tissues acquired from TCGA datasets [26]. This “limma” package was also used to analyze DEGs in SCC-9 cells treated with or without 20  $\mu$ M and prognosis-related genes of TSCC patients. Next, API-related DEGs were found

in both tissue DEGs, and prognostic genes were identified. Furthermore, API-related genes with prognostic value were selected by univariate Cox analysis of overall survival (OS). Then, interacting networks based on these API-related genes were created via the STRING database (version 11.5, developed jointly by the Swiss Institute of Bioinformatics, the Novo Nordisk Foundation Protein Research Center and the European Molecular Biology Laboratory). Aiming to create a prognostic model, Lasso Cox regression analysis further revealed target genes with the “glmnet” package. In addition, multivariate Cox analysis was also carried out to evaluate the prognostic sign of the genes. While calculating the penalty parameter ( $\lambda$ ) using the smallest possible criterion, normalized expression of the genes in TSCC patients and coefficients were gathered to analyze total risk scores. The algorithm was as follows: risk score = sum (each gene’s expression in each TSCC patient  $\times$  corresponding coefficient). Then, TSCC patients in the TCGA cohort were allocated to the high- or low-risk group as well as the Gene Expression Omnibus (GEO) cohort [27]. Principal component analysis (PCA), from running the “stats” R package, was conducted to estimate this model’s ability to isolate samples into two groups [28]. In addition, the “Rtsne” R package was run to create t-distributed stochastic neighbor embedding (t-SNE) and then further determine the groups’ distribution. For the survival analysis of each gene, the optimal cut-off expression value was determined by the “surv\_cutpoint” function of the “survminer” R package. Kaplan–Meier (K-M) analysis by the “survminer” package was built to predict the OS of TSCC patients between the high- and low-risk groups.

## 2.11 Independent Prognostic Analysis of this Model

Receiver operating characteristic (ROC) curve analysis was performed using the “survival”, “survminer”, and “timeROC” packages. The 1-year, 3-year, and 5-year OS were determined by ROC curves to estimate the anticipation capacity of the model. The relationship between clinical data acquired from the TCGA and API-related gene expression was analyzed with Cox regression analyses. Moreover, the results were visualized through forest maps.

## 2.12 Gene Set Enrichment Analysis

The input data were split into high- and low-risk groups obtained by risk scoring, and the underlying molecular pathways in API-related genes were further analyzed. Gene set enrichment analysis (GSEA) was performed by GSEA software (version 4.3.2, Broad Institute, UC San Diego, CA, USA). Simulated value = 1000,  $p$ -value < 0.05, which was conducted as the criterion for statistical significance.

## 2.13 Immune State in Diverse Risk Groups

Each sample in the high- or low-risk group was analyzed to compute the number of 22 types of immune

**Table 1. Primer sequences for qPCR.**

Variables	TCGA cohort
CASP14 (forward primer)	CTGGTGGATGTGTTACGAAGAGG
CASP14 (reverse primer)	AGGGTGCTTTGGATTCAGGGTTC
TMEM213 (forward primer)	GCAGAAGCAAGCAGCAGCAAC
TMEM213 (reverse primer)	ATCCAGCCGTA CTCTGCTCCACTC
GPR158 (forward primer)	CTGCGGAGGAGCCAAGAAAGC
GPR158 (reverse primer)	ATCTGGGTGGTGCCTGGGTTC
ITGA5 (forward primer)	CATCGCTCTCAACTTCTCCTTGGAC
ITGA5 (reverse primer)	CGGCTCTTGCTCTGATAATGTAGGG
GAPDH (forward primer)	GTCAGTGGTGGACTGACCT
GAPDH (reverse primer)	TGCTGTAGCCAAATTCGTTG

qPCR, quantitative polymerase chain reaction; TCGA, The Cancer Genome Atlas.

cells infiltrating the tumors. Furthermore, the CIBERSORT method was used to assess the correlation between patient risk scores and immune cell density [25]. The risk score was determined to explore the connection between API-related genes and 22 levels of immune cell infiltration. Additionally, between the high- and low-risk groups, the immune status and stromal scores were evaluated by the ESTIMATE algorithm [29].

#### 2.14 Drug Sensitivity Analysis

To explore drug sensitivity in the low- and high-risk groups, IC50 values of TSCC treated with multidrug treatment were determined through the “prophetic” software package.

#### 2.15 Authentication of Genes in this Signature

Based on the Human Protein Atlas, each API-related DEG used to build a prognostic model was subjected to immunohistochemistry imaging to further confirm the protein expression of these genes.

#### 2.16 Reverse Transcription-Quantitative Real-Time PCR (RT-qPCR)

Total RNA was obtained from SCC-9 cells treated with or without 20  $\mu$ M API via TRIzol (Invitrogen, Carlsbad, CA, USA). Then, complementary DNA (cDNA) was generated using the Verso complementary DNA synthesis kit (Invitrogen, Carlsbad, CA, USA). Sequences of primers for detecting target genes are described in Table 1.

#### 2.17 Statistical Analysis

During data collection, gene expression was calculated through Student’s *t*-test. Survival analysis was determined using the R survival package. In addition, the log-rank test was used to test the survival rate of each group. The Kaplan–Meier curve was utilized to predict the survival probability of the high- and low-risk groups in the data. Independent forecast factors of OS were employed through univariate and multivariate Cox regression. Moreover, the

correlation of the two subgroups in the tumor immune microenvironment, including immune cells and immune pathways, was assessed employing the Mann–Whitney test. Additionally, the correlation coefficient was measured by Spearman analysis. R version 4.1.0. (The R Foundation for Statistical Computing, Boston, MA, USA) was used for all statistical analyses, and the *p*-value was <0.05.

### 3. Results

#### 3.1 API inhibited TSCC Cell Aggressive Characteristics

To determine the API (Fig. 2A) IC50 value of the TSCC cell line, SCC-9, and CAL-27 cells were treated with API at progressively higher concentrations (0, 2, 4, 8, 16, 32, 64, 128  $\mu$ M) for 24 hours (Fig. 2B). As shown in Fig. 2B, the IC50 value was approximately 35.16  $\mu$ M in SCC-9 cells and 39.21  $\mu$ M in CAL-27 cells based on the CCK8 assay. Cell proliferation was also evaluated using the CCK8 assay (Fig. 2C,D). The effect of API on the migratory capacity of SCC-9 and CAL-27 cells was then clarified by wound-healing assay. Our data showed that API could decrease gap closure at concentrations of 20  $\mu$ M (Fig. 2E,F). Meanwhile, we also verified that API could effectively suppress cell migration and invasion by transwell assay (Fig. 2G,H). Furthermore, the colony-formation assays demonstrated that API could effectively inhibit clonogenic capacity in SCC-9 and CAL-27 cells (Fig. 2I,J). Our results show that API could markedly suppress cell proliferation, migration, and clonogenic ability of SCC-9 and CAL-27 cells.

#### 3.2 Determination of Prognostic API-Related DEGs

To explore the underlying molecular mechanism of how API restrains the malignancy of TSCC, we obtained the results of API-treated and untreated groups of DEGs through transcriptome RNA sequencing (Fig. 3A,B). Then, we also analyzed DEGs in RNA-seq data between TSCC samples and normal tissue samples from the TCGA (Fig. 3C,D). The individual information of these TSCC patients was generalized in Table 2. Integrated analy-

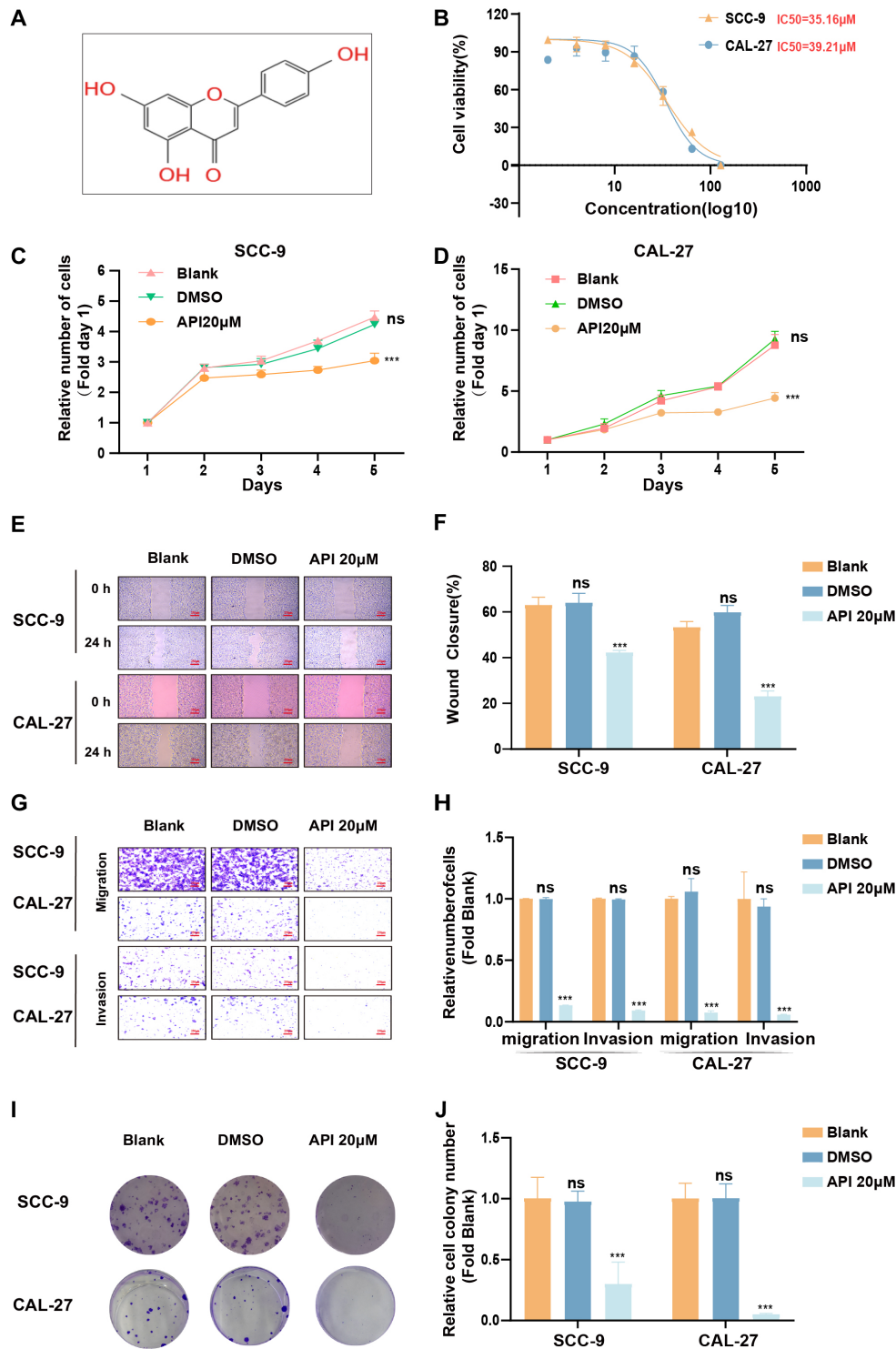


**Fig. 2. Apigenin (API) reduced Tongue squamous cell carcinoma (TSCC) cell characteristics.** (A) Chemistry architecture of API. (B) The  $IC_{50}$  value of API. The  $IC_{50}$  value was calculated by Prism 6 software. (C,D) API inhibited SCC-9 and CAL-27 cell proliferation. (E,F) API inhibited SCC-9 and CAL-27 cell migration. Typical images observed from the wound-healing assay of TSCC cells are displayed for 0 h and 24 h. (G,H) The migration and invasion ability of TSCC cells with or without API treatment in transwells. Representative photographs of transwell images were presented. (I,J) The indicated cells were seeded as single cells and maintained for 10 days. Representative photographs of colony formation were presented. The results displayed are representative of three stand-alone experiments. (F), (H), and (J) data are shown as means  $\pm$  SD (standard deviation). ns  $p > 0.05$ , \*\*\* $p < 0.001$ .

ses were performed to demonstrate relationships between DEGs in SCC-9 cells and DEGs in the RNA-seq group or the prognosis-related group with  $|\log_2(\text{fold change})| \geq 1$  and  $\text{FDR} < 0.05$  (Fig. 3E). As shown in Fig. 3E, some API-related genes were differentially expressed between normal and tumor tissue samples. Nine of them (*SLC7A14*, *ETNPPL*, *TMEM213*, *GPR158*, *GJB7*, *CASP14*, *HOXD-AS2*, *ITGA5*, and *MIR503HG*) were correlated with OS by univariate Cox regression analysis (Fig. 3F). Unexpectedly, *SLC7A14* and *ETNPPL* were downregulated in tumor samples. However, their HR expression was much higher, which can upregulate offset possibility. Consequently, these two genes were ruled out for further study. In total, 7 API-related prognostic DEGs were retained. (all  $\text{FDR} < 0.05$ , Fig. 3G). The correlation between these 7 DEGs is presented in Fig. 3H.

**Table 2. Clinical characteristics of the TSCC patients involved in this research.**

Variables	TCGA cohort
No. of patients	156
Age (years)	
<60	78 (50%)
≥60	78 (50%)
Gender (%)	
Female	50 (32.1%)
Male	106 (67.9%)
Grade	
1	20 (12.8%)
2	99 (63.4%)
3	28 (17.9%)
4	4 (2.5%)
Unknown	5 (3.1%)
Stage	
I	13 (8.3%)
II	24 (13.5%)
III	35 (22.4%)
IV	65 (41.5%)
Unknown	19 (12.1%)
Survival status	
Alive	97 (62.1%)
Dead	59 (37.8%)

TSCC, tongue squamous cell carcinoma.

### 3.3 Validation of Genes in this Prognostic Model

In the Human Protein Atlas database, only 4 genes (*CASP14*, *TMEM213*, *GPR158*, and *ITGA5*) of this prognostic model have been analyzed immunohistochemically. As displayed in Fig. 4A, the protein expression of these four genes was shown to be different in normal tissues than in tumor tissues (Fig. 4A).

To validate these 4 genes in SCC-9 cells, RT-qPCR was utilized to evaluate their mRNA expression. These SCC9 cells were treated with or without 20  $\mu\text{M}$  API for 24 hours. According to the results, *TMEM213* and *GPR158* mRNA levels were increased in the API group. In comparison with the CTRL group, the mRNA expression of *CASP14* and *ITGA5* was downregulated (Fig. 4B). In these 4 genes, *ITGA5* and *CASP14* are oncogenes, and API inhibits their expression. Since HR in *ITGA5* is much higher (Fig. 3G), we further confirmed that *ITGA5* was enhanced in tumor tissues than in paracancerous tissues through IHC (Fig. 4C).

### 3.4 Establishment and Validation of an API-Related Prognostic Model

Then, a prognostic model was constructed from the 7 genes noted above using LASSO Cox regression analysis. The risk score formula is listed below [26]:  $e(0.070 \times \text{expression level of CASP14} + 0.216 \times \text{expression level of ITGA5} + 0.212 \times \text{expression level of GPR158} + 0.319 \times \text{expression level of MIR503HG} + 1.99 \times \text{expression level of ETNPPL} + 0.214 \times \text{expression level of GJB7} + 0.309 \times \text{expression level of TMEM213})$ . In accordance with the cut-off value, the TSCC patients in the TCGA cohort were divided into two groups: a low-risk group ( $n = 74$ ) and a high-risk group ( $n = 73$ ) (Fig. 5A). In addition, high-risk patients had a higher death rate than low-risk patients (Fig. 5B). Moreover, patients in the high-risk or low-risk group were determined to be located independently via PCA and t-SNE analysis (Fig. 5C,D). The Kaplan–Meier curve steadfastly demonstrated that patients with TSCC in the low-risk category had notably better OS than those in the high-risk group (Fig. 5E,  $p < 0.001$ ).

Subsequently, to verify the reliability of the model established in the TCGA cohort, the patients from the GEO cohort were also placed in either a high- or low-risk group by the median value obtained as the same formula as that in the TCGA cohort (Fig. 5A). And from Fig. 4B, Patients in the low-risk group were more probably to own a longer OS (Fig. 5B). Similar to the outcome received from the TCGA cohort, PCA and t-SNE analysis revealed that the distribution of patients in two subgroups was in discrete directions (Fig. 5C,D). In addition, patients in the high-risk group had worse survival rates compared to the low-risk group (Fig. 5E).

After eliminating samples with inconclusive clinical information, ROC analysis was utilized to calculate AUCs. As revealed in Fig. 5F, the AUCs of the 7-gene model for 1-, 2-, and 3-year survival were 0.736, 0.718, and 0.709, respectively. The risk score was proven to be a stand-alone forecaster of OS in TSCC patients through univariate and multivariate Cox regression analyses (Fig. 5G). Then, all associated clinical factors for patients in the TCGA were used to build a predictive nomogram for OS (Fig. 5H). The red dot represents the total clinical characteristics score in

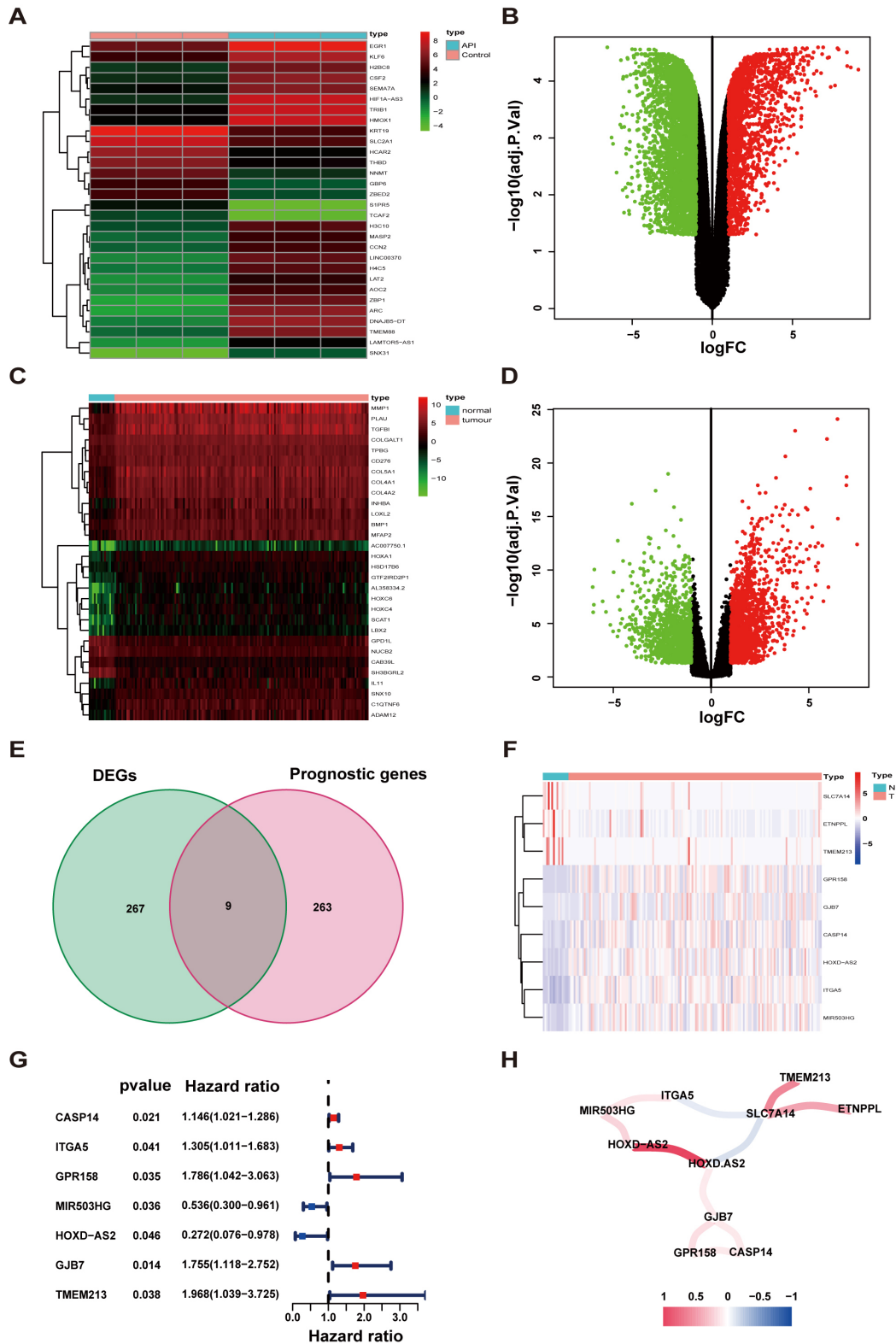


**Fig. 3. Determination of prognostic API-related differentially expressed genes (DEGs).** (A,B) Heatmap and volcano plot of API-related DEGs. (C,D) Heatmap and volcano plot of TSCC-related DEGs. (E) Venn diagram to determine API-related DEGs that were associated with overall survival (OS). (F) The expression of 9 overlaying key genes in tissues. (G) Through univariate Cox regression analysis, Forest plots display the relationship between OS and gene expression. (H) The network of prognostic API-related genes (red and blue lines represent positive and negative relativities, respectively). Darker colors represent stronger associations. FC, fold change.

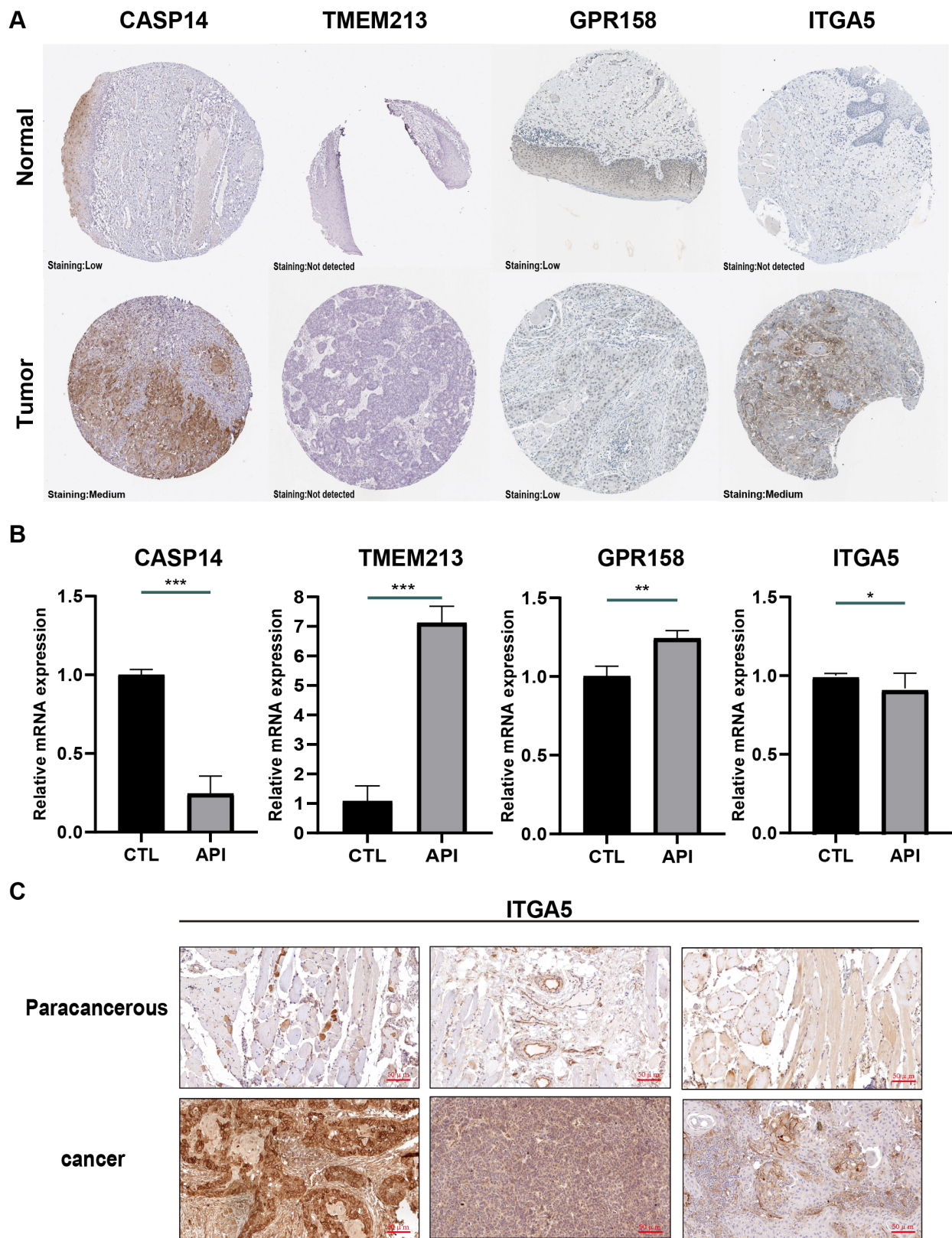


**Fig. 4. Validation of genes in this prognostic model.** (A) Immunohistochemistry results of tissue samples from the Human Protein Atlas database (image available from [v15.proteinatlas.org](http://v15.proteinatlas.org)). (B) mRNA levels of caspase 14 (CASP14), transmembrane protein 213 (TMEM213), G protein-coupled receptor 158 (GPR158), integrin subunit alpha 5 (ITGA5) in SCC-9 cells. (\* $p < 0.05$ , \*\* $p < 0.01$  and \*\*\* $p < 0.001$ , compared with the control group). (C) Representative immunohistochemical images of ITGA5 expression in primary TSCC cancer tissues and normal aracancerous tissue. Scale bar, 50  $\mu$ M.

a TSCC patient from the TCGA, which is 263 points. This red dot also indicates that the survival probabilities in this patient for 1, 3, and 5 years were 85.4, 69.5, and 53.2%, respectively. The 1-, 3-, and 5-year OS of TSCC patients were also evaluated using calibration curves (Fig. 5I).

### 3.5 Functional Analysis Based on the Prognostic Model

Aiming to determine the function of API-related prognostic genes, GSEA was utilized to diagnose relative underlying pathways between the low- and high-risk groups. Based on the results, the enriched pathways in the high-risk group were mostly specialized in focal adhesion, ECM receptor interaction, viral myocarditis, regulation of actin cytoskeleton, leishmania infection, and coagulation cascades (Fig. 6A). The enriched mechanisms of the low-risk group were Parkinson's disease, oxidative phosphorylation, Huntington's disease, Alzheimer's disease, seven amino acid metabolism, and one carbon pool by folate (Fig. 6B).

### 3.6 Relationship between Risk Score and TME or Drug Susceptibility

As shown in Fig. 7A, the risk score was linked to regulatory T cells (Tregs), follicular helper T cells, CD8 T cells, resting mast cells, memory B cells, and M1 macrophages (Fig. 7A). In addition, a correlation between the 7 genes and the number of immune cells was also observed. The results showed that some immune cells were easily affected by these 7 genes (Fig. 7B). Additionally, T cells can be inhibited by stromal activation of the TME. The tumor stroma and ESTIMATE scores were much lower in the low-risk group than in the high-risk group (Fig. 7C).

A drug susceptibility test was performed to analyze the effect of anticancer drugs in different risk groups. In the high-risk group, the results indicated that the IC50 values of bexarotene, bicalutamide, pazopanib, and WO2009093972 were much lower. The chemotherapeutic agents in the high-risk group, including A443654 and vinorelbine, had higher IC50 values than those in the low-risk group (Fig. 7D).

## 4. Discussion

Previous studies have demonstrated that API has various biological functions, including antitumor, anti-inflammatory, and antioxidant activities [30]. Regarding antitumor function, a recent study pointed out that API could induce apoptosis in the A431 cell line by downregulating sulfiredoxin expression [31]. In addition, in the KRAS-mutant NSCLC model, API could effectively reduce the proliferation ability [32]. Moreover, under hypoxic conditions in gastric cancer cells, API initiates autophagic cell death through inhibition of HIF-1 $\alpha$  and Ezh2 expression [33]. Despite the antitumor effect of API having been demonstrated in various cancers, the effect of API in TSCC has not been well-proven.

In the present work, we first proved that API can efficiently reduce cell proliferation and migration in TSCC

cells, which provides new drug options for clinical treatment. Then, through RNA-seq data and the GEO database, we identified 7 key API-related prognostic genes (*CASP14*, *TMEM213*, *GPR158*, *MIR503HG*, *HOXD-AS2*, *GJB7*, and *ITGA5*). These genes all displayed potential as prognostic biomarkers. In terms of *CASP14*, alterations in *CASP14* expression could lead to tumor pathogenesis and progression [33]. It was discovered that *CASP14* expression was decreased in some malignant cancers. In addition, high expression of *TMEM213* could promote the development of renal cell carcinoma [34]. Regarding *GPR158*, a study revealed that *GPR158* is essential in prostate cancer growth and progression [35]. In vascular disease, *MIR503HG* deficiency enhanced the conversion of endothelial cells to mesenchymal cells [36]. *In vivo*, silencing of lncRNA *HOXD-AS2* prevents glioma cell proliferation, and its expression level relates to tumor grade and prognosis in GBM [37]. Additionally, *GJB7* was found to be mutated in gastric and colorectal cancers [38]. *ITGA5*, a member of the integrin alpha chain family, has been shown to function in promoting cancer cell infiltration and migration [39]. In breast cancer, high expression of *ITGA5* in tumor cell-derived extracellular vesicles can increase metastasis probability [40]. In our research, *ITGA5* was performed as an oncogene with higher HR value and elevated in TSCC tumor tissues compared to paraneoplastic tissues of patients. Previous studies show that *ITGA5* could effectively promote TSCC cell proliferation and migration [41], which is consistent with our findings.

Next, we demonstrated a novel independent prognostic model based on these 7 key API-related prognostic genes. At present, there are some other prognostic models for TSCC patients. Prognostic models incorporating age, tumor nodal metastasis (TNM) stage, erythrocytes, platelets, and platelet-to-lymphocyte ratios can be effective in improving the accuracy of OS prediction for TSCC [42]. Besides, prognostic models that include the variables of inflammatory response, tumor outgrowth, and depth of infiltration are strongly associated with TSCC lymph node metastasis and recurrence and can be used as predictors of survival in patients with TSCC [43]. Additionally, some researchers have developed prognostic models using 11 key predictor genes through Cox and LASSO analysis of The Cancer Genome Atlas and the GSE65858 database (on overall survival) [44]. The risk model had a better prognosis than other clinical features. However, there are no prognostic models in TSCC that incorporate treatment-associated genes into the construct system at this time. We integrated API-associated genes into the TSCC prognostic modeling system, which can better evaluate the ability of API to influence the prognosis of patients. Our study also found that the risk score based on this prognostic model was closely correlated with immune cells and the TME, which means that API may inhibit SCC-9 cellular activity by affecting immune cells. The TME, composed of various cellular and

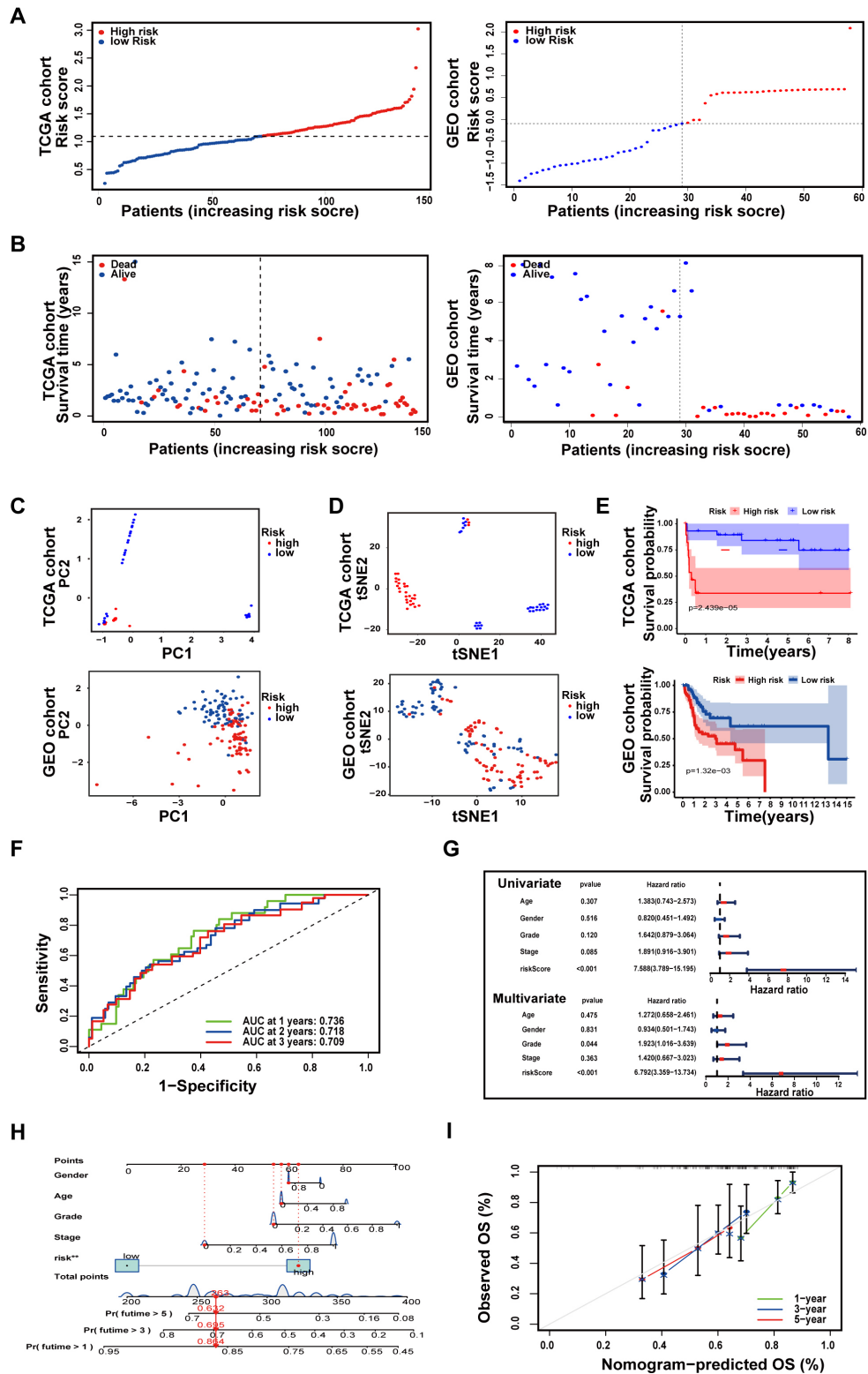


**Fig. 5. Establishment and Validation of an API-related prognostic model.** (A) The distribution of TSCC patients with risk scores in the The Cancer Genome Atlas (TCGA) cohort and Gene Expression Omnibus (GEO) cohort. (B) The locations and OS status of TSCC patients with different risk scores in the TCGA cohort and GEO cohort. (C) Principal component analysis (PCA) plot of the prognostic model. (D) t-SNE analysis of the prognostic model. (E) Kaplan–Meier survival curve of TSCC patients. (F) ROC curves demonstrate the predictive validity of risk scores. (G) Forest plots for univariate and multivariate Cox regression analysis of patients in TCGA. (H) Nomogram predicting 1-, 2-, and 3-year OS in TSCC patients. (I) Calibration curves for consistency testing between forecasted and real OS.

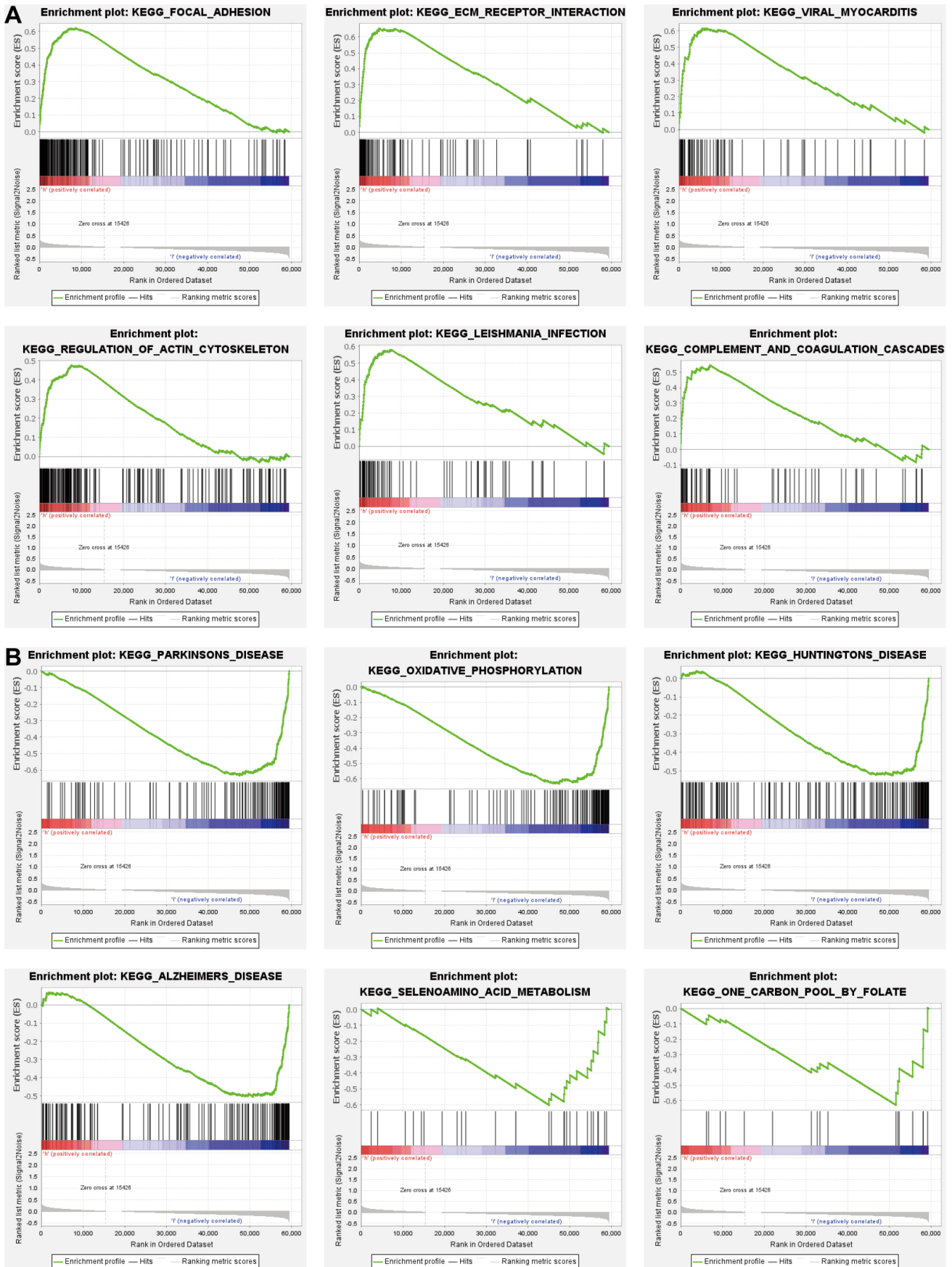


**Fig. 6. Functional analysis based on the prognostic model. (A,B) Mechanisms dramatically enriched in high- (A) and low-risk groups (B) through gene set enrichment analysis (GSEA).**

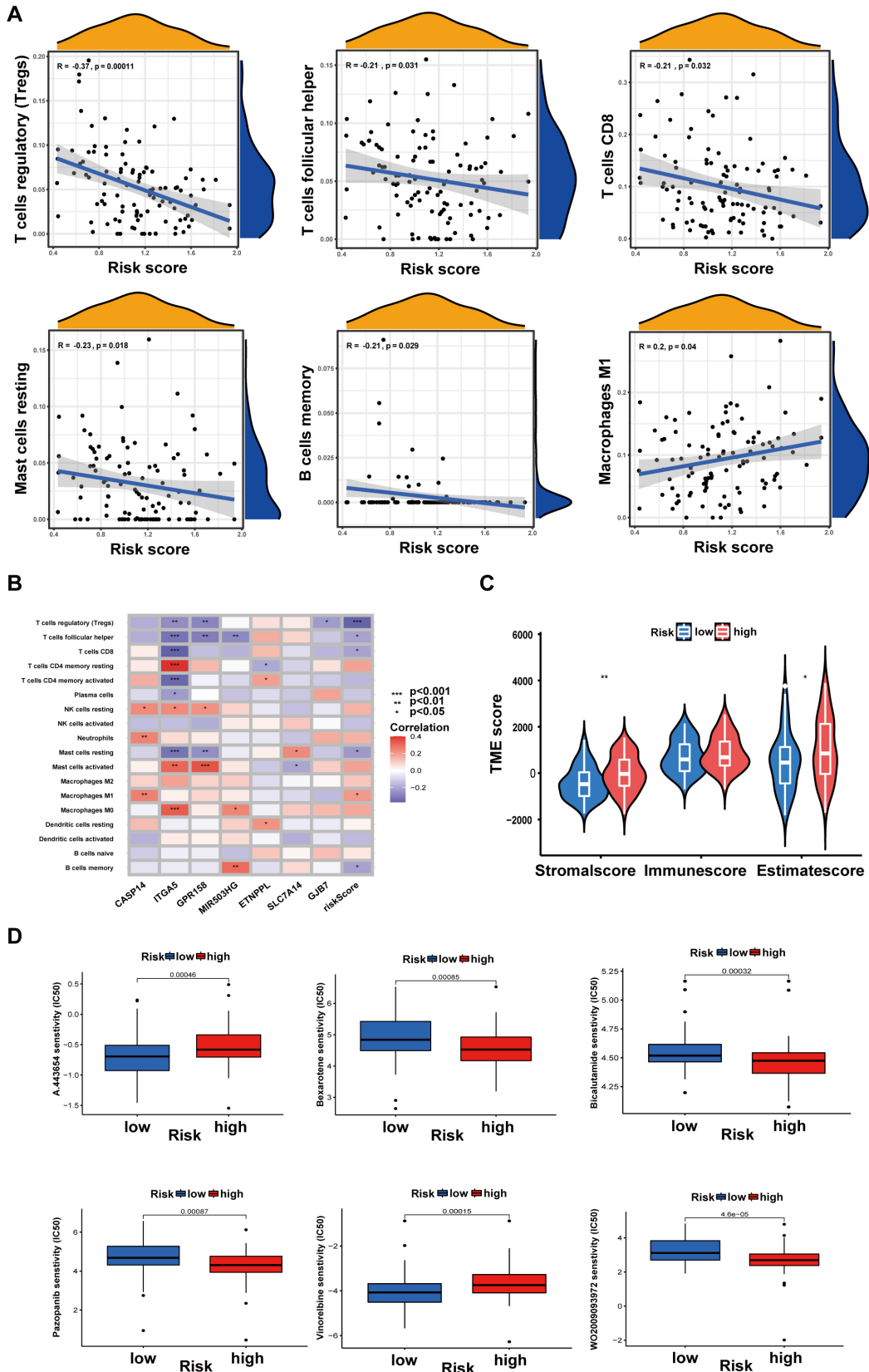


**Fig. 7. Relationship between risk score and tumor microenvironment (TME) or Drug susceptibility.** (A) Relations between risk score and immune cell types. (B) Seven genes in the prognostic model were associated with the number of immune cells. (C) Relationships between risk score and TME scores. (D) Drug susceptibility. Data are shown as the mean  $\pm$  SD. (\* $p < 0.05$ , \*\* $p < 0.01$  and \*\*\* $p < 0.001$ ).

noncellular actors, has been demonstrated to impact cancer progression and the outcomes of cancer therapy [45]. Cancer immune escape is an active process that regulates immune responses with the help of immunosuppressive cells [46,47]. And TSCC patients mostly suffer from CD8<sup>+</sup> T or Foxp3<sup>+</sup> regulatory T-cell (Treg) infiltration [45]. Moreover, patients in diverse risk groups showed a difference in their sensitivity to drug treatment, which can provide beneficial insight for developing treatment strategies combining API and other drugs and bring hopeful prognostic outcomes.

In summary, several limitations were present in this study. First, the data in this research were mostly obtained from TCGA databases, and more real-world data are needed to validate their accuracy. Second, the API-associated genes obtained in this study that can guide TSCC prognosis, immune microenvironment, and combination drug therapy need to be further investigated for their biological functions.

## 5. Conclusions

In conclusion, our research validated the efficacy of API in inhibiting cancer progression using *in vitro* experiments. Furthermore, we incorporated therapeutic factors with disease occurrence and progression factors to construct a fusion of innovative prognostic models for TSCC tumor patients. The API-related prognostic model was well-predicting patient OS and the immunological status of the TME. In addition to API, we identified six drugs that may be potentially efficacious in the treatment of TSCC. The results of this study have the potential to improve clinical outcomes and overall survival in patients with TSCC.

## Abbreviations

TSCC, Tongue squamous cell carcinoma; API, Apigenin; DEGs, differentially expressed genes; ROC, Receiver operating characteristic; TCGA, The Cancer Genome Atlas; TME, tumor microenvironment; ATCC, American Type Culture Collection; IC50, The semi-inhibitory concentration; CCK-8, the Cell Counting Kit-8; FDR, false discovery rate; OS, overall survival; PCA, Principal component analysis; t-SNE, t-distributed stochastic neighbor embedding; GEO, the Gene Expression Omnibus; M, Kaplan–Meier; FBS, fetal bovine serum; IHC, Immunohistochemistry; GSEA, Gene set enrichment analysis; cDNA, complementary DNA.

## Availability of Data and Materials

The datasets generated and/or analysed during the current study are available in the Gene Expression Omnibus database (<https://www.ncbi.nlm.nih.gov/geo/>); [GEO accession: GSE111395 (<https://www.ncbi.nlm.nih.gov/geo/query/acc.cgi?acc=GSE111395>), and GSE75540 (<https://www.ncbi.nlm.nih.gov/geo/query/acc.cgi?acc=GSE75540>)].

## Author Contributions

FQ designed the study. JL and CF made contributions to the data analyses. JL drew up the manuscript. GZ and CS accomplished statistical analysis for the data. FY and WG conducted molecular experiments. JD performed the experimentation on animals. JX and CL processed figures and tables. FQ undertook support for the project. All authors have browsed and agreed with the final manuscript. All authors contributed to editorial changes in the manuscript. And all authors have participated sufficiently in the work and agreed to be accountable for all aspects of the work.

## Ethics Approval and Consent to Participate

This study has been reviewed and approved by the ethics institution committee of Gaoxin Branch of the First Affiliated Hospital of Nanchang University (No. [2024]01), Nanchang, China, and compliance with the declaration of Helsinki.

## Acknowledgment

Not applicable.

## Funding

This study was supported by the grants from National Natural Science Foundation of China (No. 81960495), the Jiangxi Provincial Natural Science Foundation (No. 20212ACB206029), and the Nanchang Key Laboratory of Tumor Gene Diagnosis and Innovative Treatment Research (No. 2021-NCZDSY-009).

## Conflict of Interest

The authors declare no conflict of interest.

## References

- [1] Gupta S, Afaq F, Mukhtar H. Selective growth-inhibitory, cell-cycle deregulatory and apoptotic response of apigenin in normal versus human prostate carcinoma cells. *Biochemical and Biophysical Research Communications*. 2001; 287: 914–920.
- [2] Singh P, Mishra SK, Noel S, Sharma S, Rath SK. Acute exposure of apigenin induces hepatotoxicity in Swiss mice. *PLoS ONE*. 2012; 7: e31964.
- [3] Salehi B, Venditti A, Sharifi-Rad M, Kręgiel D, Sharifi-Rad J, Durazzo A, *et al*. The Therapeutic Potential of Apigenin. *International Journal of Molecular Sciences*. 2019; 20: 1305.
- [4] Plumb J, Pigat S, Bompola F, Cushen M, Pinchen H, Nørby E, *et al*. eBASIS (Bioactive Substances in Food Information Systems) and Bioactive Intakes: Major Updates of the Bioactive Compound Composition and Beneficial Bioeffects Database and the Development of a Probabilistic Model to Assess Intakes in Europe. *Nutrients*. 2017; 9: 320.
- [5] Pápay ZE, Kósa A, Böddi B, Merchant Z, Saleem IY, Zariwala MG, *et al*. Study on the Pulmonary Delivery System of Apigenin-Loaded Albumin Nanocarriers with Antioxidant Activity. *Journal of Aerosol Medicine and Pulmonary Drug Delivery*. 2017; 30: 274–288.
- [6] Wang YC, Huang KM. *In vitro* anti-inflammatory effect of apigenin in the *Helicobacter pylori*-infected gastric adenocarcinoma cells. *Food and Chemical Toxicology: an International*

Journal Published for the British Industrial Biological Research Association. 2013; 53: 376–383.

- [7] Caltagirone S, Rossi C, Poggi A, Ranelletti FO, Natali PG, Brunetti M, *et al.* Flavonoids apigenin and quercetin inhibit melanoma growth and metastatic potential. *International Journal of Cancer*. 2000; 87: 595–600.
- [8] Wang W, Heideman L, Chung CS, Pelling JC, Koehler KJ, Birt DF. Cell-cycle arrest at G2/M and growth inhibition by apigenin in human colon carcinoma cell lines. *Molecular Carcinogenesis*. 2000; 28: 102–110.
- [9] Cheng Y, Han X, Mo F, Zeng H, Zhao Y, Wang H, *et al.* Apigenin inhibits the growth of colorectal cancer through down-regulation of E2F1/3 by miRNA-215-5p. *Phytomedicine: International Journal of Phytotherapy and Phytopharmacology*. 2021; 89: 153603.
- [10] Pham TH, Page YL, Percevault F, Ferrière F, Flouriot G, Pakdel F. Apigenin, a Partial Antagonist of the Estrogen Receptor (ER), Inhibits ER-Positive Breast Cancer Cell Proliferation through Akt/FOXMI Signaling. *International Journal of Molecular Sciences*. 2021; 22: 470.
- [11] Birt DF, Mitchell D, Gold B, Pour P, Pinch HC. Inhibition of ultraviolet light induced skin carcinogenesis in SKH-1 mice by apigenin, a plant flavonoid. *Anticancer Research*. 1997; 17: 85–91.
- [12] Mirzoeva S, Tong X, Bridgeman BB, Plebanek MP, Volpert OV. Apigenin Inhibits UVB-Induced Skin Carcinogenesis: The Role of Thrombospondin-1 as an Anti-Inflammatory Factor. *Neoplasia (New York, N.Y.)*. 2018; 20: 930–942.
- [13] Maggioni D, Garavello W, Rigolio R, Pignataro L, Gaini R, Nicolini G. Apigenin impairs oral squamous cell carcinoma growth *in vitro* inducing cell cycle arrest and apoptosis. *International Journal of Oncology*. 2013; 43: 1675–1682.
- [14] Vigneswaran N, Williams MD. Epidemiologic trends in head and neck cancer and aids in diagnosis. *Oral and Maxillofacial Surgery Clinics of North America*. 2014; 26: 123–141.
- [15] Zhang T, Liang L, Liu X, Wu JN, Chen J, Su K, *et al.* TGF $\beta$ 1-Smad3-Jagged1-Notch1-Slug signaling pathway takes part in tumorigenesis and progress of tongue squamous cell carcinoma. *Journal of Oral Pathology & Medicine: Official Publication of the International Association of Oral Pathologists and the American Academy of Oral Pathology*. 2016; 45: 486–493.
- [16] Bello IO, Soini Y, Salo T. Prognostic evaluation of oral tongue cancer: means, markers and perspectives (I). *Oral Oncology*. 2010; 46: 630–635.
- [17] J Caudell JJ, Gillison ML, Maghami E, Spencer S, Pfister DG, Adkins D, *et al.* NCCN Guidelines® Insights: Head and Neck Cancers, Version 1.2022. *Journal of the National Comprehensive Cancer Network*. 2022; 20: 224–234.
- [18] Sasahira T, Bosserhoff AK, Kirita T. The importance of melanoma inhibitory activity gene family in the tumor progression of oral cancer. *Pathology International*. 2018; 68: 278–286.
- [19] Huang W, Zhou X, Liao Q, Tang Y, Zuo L, Wang H, *et al.* Clinicopathological and prognostic significance of PD-1/PD-L1 axis expression in patients with tongue squamous cell carcinoma. *Journal of Cellular Physiology*. 2020; 235: 6942–6953.
- [20] Sun L, Liang J, Wang Q, Li Z, Du Y, Xu X. MicroRNA-137 suppresses tongue squamous carcinoma cell proliferation, migration and invasion. *Cell Proliferation*. 2016; 49: 628–635.
- [21] Klatte T, Rossi SH, Stewart GD. Prognostic factors and prognostic models for renal cell carcinoma: a literature review. *World Journal of Urology*. 2018; 36: 1943–1952.
- [22] Repo H, Löyttyniemi E, Kurki S, Kallio L, Kuopio T, Talvinen K, *et al.* A prognostic model based on cell-cycle control predicts outcome of breast cancer patients. *BMC Cancer*. 2020; 20: 558.
- [23] Park HS, Park JS, Chun YJ, Roh YH, Moon J, Chon HJ, *et al.* Prognostic Factors and Scoring Model for Survival in Metastatic Biliary Tract Cancer. *Cancer Research and Treatment*. 2017; 49: 1127–1139.
- [24] Choi Y, Oh DY, Park H, Kim TY, Lee KH, Han SW, *et al.* More Accurate Prediction of Metastatic Pancreatic Cancer Patients' Survival with Prognostic Model Using Both Host Immunity and Tumor Metabolic Activity. *PloS One*. 2016; 11: e0145692.
- [25] D Hou, J-N Tan, S-N Zhou, X Yang, Z-H Zhang, G-Y Zhong, *et al.* A novel prognostic signature based on cuproptosis-related lncRNA mining in colorectal cancer. *Frontiers in Genetics*. 2022; 13: 969845.
- [26] Liang JY, Wang DS, Lin HC, Chen XX, Yang H, Zheng Y, *et al.* A Novel Ferroptosis-related Gene Signature for Overall Survival Prediction in Patients with Hepatocellular Carcinoma. *International Journal of Biological Sciences*. 2020; 16: 2430–2441.
- [27] Jiang F, Miao XL, Zhang XT, Yan F, Mao Y, Wu CY, *et al.* A Hypoxia Gene-Based Signature to Predict the Survival and Affect the Tumor Immune Microenvironment of Osteosarcoma in Children. *Journal of Immunology Research*. 2021; 2021: 5523832.
- [28] Qian H, Lei T, Hu Y, Lei P. Expression of Lipid-Metabolism Genes Is Correlated with Immune Microenvironment and Predicts Prognosis in Osteosarcoma. *Frontiers in Cell and Developmental Biology*. 2021; 9: 673827.
- [29] Mithani SK, Mydlarz WK, Grumbine FL, Smith IM, Califano JA. Molecular genetics of premalignant oral lesions. *Oral Diseases*. 2007; 13: 126–133.
- [30] Kim HY, Kim OH, Sung MK. Effects of phenol-depleted and phenol-rich diets on blood markers of oxidative stress, and urinary excretion of quercetin and kaempferol in healthy volunteers. *Journal of the American College of Nutrition*. 2003; 22: 217–223.
- [31] Jiang ZB, Wang WJ, Xu C, Xie YJ, Wang XR, Zhang YZ, *et al.* Luteolin and its derivative apigenin suppress the inducible PD-L1 expression to improve anti-tumor immunity in KRAS-mutant lung cancer. *Cancer Letters*. 2021; 515: 36–48.
- [32] Kim TW, Lee HG. Apigenin Induces Autophagy and Cell Death by Targeting EZH2 under Hypoxia Conditions in Gastric Cancer Cells. *International Journal of Molecular Sciences*. 2021; 22: 13455.
- [33] Krajewska M, Kim H, Shin E, Kennedy S, Duffy MJ, Wong YF, *et al.* Tumor-associated alterations in caspase-14 expression in epithelial malignancies. *Clinical Cancer Research: an Official Journal of the American Association for Cancer Research*. 2005; 11: 5462–5471.
- [34] Wrzesiński T, Szlag M, Cieślowski WA, Ida A, Giles R, Zdro E, *et al.* Expression of pre-selected TMEMs with predicted ER localization as potential classifiers of ccRCC tumors. *BMC Cancer*. 2015; 15: 518.
- [35] Fenner A. Prostate cancer: Orphan receptor GPR158 finds a home in prostate cancer growth and progression. *Nature Reviews. Urology*. 2015; 12: 182.
- [36] Monteiro JP, Rodor J, Caudrillier A, Scanlon JP, Spiroski AM, Dudnakova T, *et al.* MIR503HG Loss Promotes Endothelial-to-Mesenchymal Transition in Vascular Disease. *Circulation Research*. 2021; 128: 1173–1190.
- [37] Zhong X, Cai Y. Long non-coding RNA (lncRNA) HOXD-AS2 promotes glioblastoma cell proliferation, migration and invasion by regulating the miR-3681-5p/MALT1 signaling pathway. *Bioengineered*. 2021; 12: 9113–9127.
- [38] Son HJ, An CH, Yoo NJ, Lee SH. Tight Junction-Related CLDN5 and CLDN6 Genes, and Gap Junction-Related GJB6 and GJB7 Genes Are Somatic Mutated in Gastric and Colorectal Cancers. *Pathology Oncology Research: POR*. 2020; 26: 1983–1987.
- [39] Zhu H, Wang G, Zhu H, Xu A. ITGA5 is a prognostic biomarker and correlated with immune infiltration in gastrointestinal tu-

mors. BMC Cancer. 2021; 21: 269.

- [40] Li XQ, Zhang R, Lu H, Yue XM, Huang YF. Extracellular Vesicle-Packaged CDH11 and ITGA5 Induce the Premetastatic Niche for Bone Colonization of Breast Cancer Cells. *Cancer Research*. 2022; 82: 1560–1574.
- [41] Li T, Wu Q, Liu D, Wang X. miR-27b Suppresses Tongue Squamous Cell Carcinoma Epithelial-Mesenchymal Transition by Targeting ITGA5. *OncoTargets and Therapy*. 2020; 13: 11855–11867.
- [42] Wei LF, Huang XC, Lin YW, Luo Y, Ding TY, Liu CT, *et al.* A Prognostic Model Based on Clinicopathological Features and Inflammation- and Nutrition-Related Indicators Predicts Overall Survival in Surgical Patients with Tongue Squamous Cell Carcinoma. *Technology in Cancer Research & Treatment*. 2021; 20: 15330338211043048.
- [43] Yu P, Wang W, Zhuang Z, Xie N, Xu J, Wang C, *et al.* A novel prognostic model for tongue squamous cell carcinoma based on the characteristics of tumour and its microenvironment: iBD score. *Histopathology*. 2019; 74: 766–779.
- [44] Jin Y, Wang Z, Tang W, Liao M, Wu X, Wang H. An Integrated Analysis of Prognostic Signature and Immune Microenvironment in Tongue Squamous Cell Carcinoma. *Frontiers in Oncology*. 2022; 12: 891716.
- [45] Xiao Y, Yu D. Tumor microenvironment as a therapeutic target in cancer. *Pharmacology & Therapeutics*. 2021; 221: 107753.
- [46] Bader JE, Voss K, Rathmell JC. Targeting Metabolism to Improve the Tumor Microenvironment for Cancer Immunotherapy. *Molecular Cell*. 2020; 78: 1019–1033.
- [47] Vitale I, Manic G, Coussens LM, Kroemer G, Galluzzi L. Macrophages and Metabolism in the Tumor Microenvironment. *Cell Metabolism*. 2019; 30: 36–50.